



Optimization Mechanisms of Microstructure and Mechanical Properties of SiC Fiber Reinforced Ti/Al₃Ti Laminated Composite Synthesized Using Titanium Barrier

Chunfa Lin¹ · Siyu Wang¹ · Haoran Yan¹ · Yuqiang Han¹ · Junyi Zhu¹ · Hao Shi¹

Received: 2 March 2020 / Accepted: 1 April 2020 / Published online: 11 May 2020
© The Korean Institute of Metals and Materials 2020

Abstract

A novel structure-optimized SiC fiber reinforced metal-intermetallic-laminated composite (SiC_f-Ti/Al₃Ti) without intermetallic centerline defect has been fabricated by vacuum hot pressing using stacked fibers and foils as well as Ti barrier layer. Through microstructure characterization by SEM and EBSD, the mechanisms of centerline formation and structural optimization were investigated detailedly. The mechanical properties and fracture behaviors of the optimized and non-optimized SiC_f-Ti/Al₃Ti composites were studied via quasi-static compression tests. The experimental results indicated that the intermetallic centerline region existing at the mid-plane of Al₃Ti layer in non-optimized composite mainly contains newly-formed Kirkendall voids and gathered metallic oxides. Additionally, owing to the similar moving trails of fibers, oxides and voids in molten Al during hot pressing, SiC fiber is always accompanied with centerline, which causes the poor bonding of SiC_f/Al₃Ti interface. Unlike that, due to the adding of Ti barrier layer, SiC fibers are separated from centerline and metallurgically bonded with Al₃Ti intermetallic in the optimized composite. The compression testing results proved that the optimized SiC_f-Ti/Al₃Ti composite possesses superior strength and toughness compared with those of the non-optimized composite. Besides, the extending of cracks along centerline often leads to large-scale centerline splitting and untimely SiC_f/Al₃Ti interface debonding in non-optimized composite. Nevertheless, cracks formed in optimized composite tend to propagate at the interfacial zone between layers instead of cutting off Al₃Ti layer along its mid-plane. Moreover, ascribed to the well-bonded SiC_f/Al₃Ti interface, SiC fibers play an important role in strengthening and toughening the optimized SiC_f-Ti/Al₃Ti composite by fiber bridging mechanism.

Keywords Laminated composite · Intermetallic centerline · Interfacial bond · Structure optimization · Performance improvement

1 Introduction

Recently, metal-intermetallic-laminated (MIL) composites are considered as potential candidate structural material for using in aerospace and automotive industries because of their unique multilayered structure and excellent mechanical properties [1–4]. Especially, Ti/Al₃Ti laminates have been the research focus of MIL composites in the last two decades due to the superior comprehensive performance than those of other MIL composites, such as higher specific strength

and specific stiffness [5–8]. However, the practical application of Ti/Al₃Ti composite sheet is still a challenge in view of the limited ductility and poor toughness of Al₃Ti intermetallic at room temperature. Thus, a method of introducing fiber reinforcement into intermetallic layer of Ti/Al₃Ti laminate has been developed to manufacture novel ceramic-fiber-reinforced metal-intermetallic-laminated (CFR-MIL) composites, in which Al₃Ti intermetallic is toughening by metal layers as well as ceramic fibers [9–11].

The CFR-MIL composite is comprised of alternative Ti layers and ceramic fiber reinforced Al₃Ti layers, and the fibers are usually arranged regularly at the mid-planes of Al₃Ti layers as reported in previous works [12–14]. For instance, Vecchio et al. [13] synthesized Ti-Al₃Ti-Al₂O₃-Al CFR-MIL composite via reactive foil sintering using Al₂O₃/Al “met-preg” tapes. The investigation results demonstrated that the

✉ Yuqiang Han
hanyuqiang@cslg.edu.cn

¹ School of Materials Engineering, Changshu Institute of Technology, Changshu 215500, China

Al_2O_3 fibers, oriented in 0° and 90° layers in this composite, can arrest cracks formed in brittle Al_3Ti phase and have a considerable toughening effect. Moreover, $\text{SiC}_f\text{-Ti}/\text{Al}_3\text{Ti}$ CFR-MIL composite was studied preliminarily associated with its microstructure and mechanical properties [14]. It was suggested through compression and bending tests that $\text{SiC}_f\text{-Ti}/\text{Al}_3\text{Ti}$ CFR-MIL composite possesses higher strength and toughness than those of MIL composite without fiber reinforcement. Furthermore, molybdenum metal fiber and NiTi shape memory alloy (SMA) fiber have also been selected to prepare fiber-reinforced MIL composites, which exhibit excellent comprehensive performances [15, 16].

Currently, various CFR-MIL composites are usually synthesized by reactive foil sintering [17], spark plasma sintering [18], roll bonding sintering [1] and explosive welding [7] techniques. Compared with other techniques, reactive foil sintering has many advantages, such as obtaining well-bonded interface between layers, achieving nearly full-density intermetallic microstructure. Besides, it is easy to tailor the composition, layer thickness and phase volume fraction of the component simply through varying the category and thickness of initial foils. However, the intermetallic centerline, as a microstructural deficiency, is formed unavoidably in the laminated composite produced using this approach [5, 11, 15]. Li et al. [19] studied the failure behavior of $\text{Ti}/\text{Al}_3\text{Ti}$ MIL composite detailedly by compression tests. The results showed that when loaded, brittle cracks are usually formed at centerline zone and then propagate along this area, causing the inter delamination at the mid-plane of intermetallic layer. This phenomenon proved that the centerline is much weaker than the other part of the composite. Additionally, the previously reported work [12] indicated that in CFR-MIL composite, the formation of centerline has a strong negative impact to the bonding of interface between fiber reinforcement and intermetallic matrix, limiting the fiber toughening effect. Price et al. [20] noted that the forming of centerline is attributed to the gathering of oxides in center area of Al_3Ti layer, which come from the surface of raw foils. They also proposed a method of remaining moderate amount of unreacted Al at the mid-plane of Al_3Ti layer in $\text{Ti}/\text{Al}_3\text{Ti}$ MIL composite. The result indicated that due to the existence of residual Al served as a ductile reinforcement, the mechanical properties of $\text{Ti}/\text{Al}_3\text{Ti}$ laminate are increased. However, the residual Al phase will lead to the reduction in strength and modulus of the composite. Additionally, this method is not suitable for $\text{SiC}_f\text{-Ti}/\text{Al}_3\text{Ti}$ CFR-MIL composite because the reaction between Al phase and SiC fiber can easily cause fiber degradation. Besides, the CFR-MIL composite synthesized using initial foils, whose surfaces were strictly grounded and cleaned, still exhibited intermetallic centerline [14]. Obviously, except for the oxides, the centerline may be formed by some other mechanisms. Han et al. [21] prepared CFR-MIL composite using NiTi fiber as reaction

component. In this material, centerline is successfully eliminated ascribed to the unique NiTi-Al reaction mechanism. Nevertheless, the newly-generated Al_3Ni phase increases the density of CFR-MIL composite, and the addition of NiTi fiber raises the cost of raw materials. Hence, it is fascinating to ascertain the formation mechanism of intermetallic centerline and seek out proper approaches for weakening or even eliminating the centerline as well as its influence on the performance of CFR-MIL composite.

In the present work, vacuum hot pressing sintering method was employed to prepare $\text{SiC}_f\text{-Ti}/\text{Al}_3\text{Ti}$ CFR-MIL composite using stacked Al foils, Ti foils and SiC fibers. Besides, thin titanium sheet was added into initial stacks as barrier layer between SiC fiber and Al foil to obtain a structure-optimized $\text{SiC}_f\text{-Ti}/\text{Al}_3\text{Ti}$ composite. Initially, microstructures of the optimized and non-optimized CFR-MIL composites were investigated via SEM, EDS, EBSD and XRD. The mechanical properties of these two composites were detected by quasi-static compression tests. Then, the basic theory of centerline formation in CFR-MIL composite was discussed detailedly. Finally, the improvement mechanisms of microstructure and properties of the optimized CFR-MIL composite were clarified.

2 Experimental Procedures

2.1 Materials and Processing

In this work, $\text{SiC}_f\text{-Ti}/\text{Al}_3\text{Ti}$ CFR-MIL composite was fabricated by vacuum hot pressing using titanium foil (500 μm thick, TA1), aluminum foil (600 μm thick, 1060Al) and SiC fiber (12 μm in diameter) as raw materials. Before sintering, the as-received metal foils were ground using silicon carbide paper to dislodge surface oxides and impurities. Subsequently, both the foils and SiC fibers were cleaned in water bath, rinsed using alcohol and dried in sequence. After these procedures, the foils and fibers were stacked alternately into foil-fiber-foil laminates with titanium top and bottom, as shown in Fig. 1. It can be seen that two kinds of stack units were designed: “Ti-SiC_f-Al-SiC_f-Ti” unit for preparing non-optimized CFR-MIL composite, and “Ti-Al-Ti_{barrier}-SiC_f-Ti_{barrier}-Al-Ti” unit with Ti barrier sheet (100 μm thick, TA1) placed between SiC fiber and Al foil to obtain structure-optimized composite. Then, the laminates comprised of three stack units were sintered at 660 °C for 4 h in hot press sintering furnace at high vacuum ($\sim 10^{-3}$ Pa), as shown in Fig. 1a and b. Loading pressures of 2.5 MPa was applied on the laminates during most of the reaction period except for Al melting. The synthesized composite was cooled down to room temperature with the furnace. Typical hot-pressing processing parameters of the

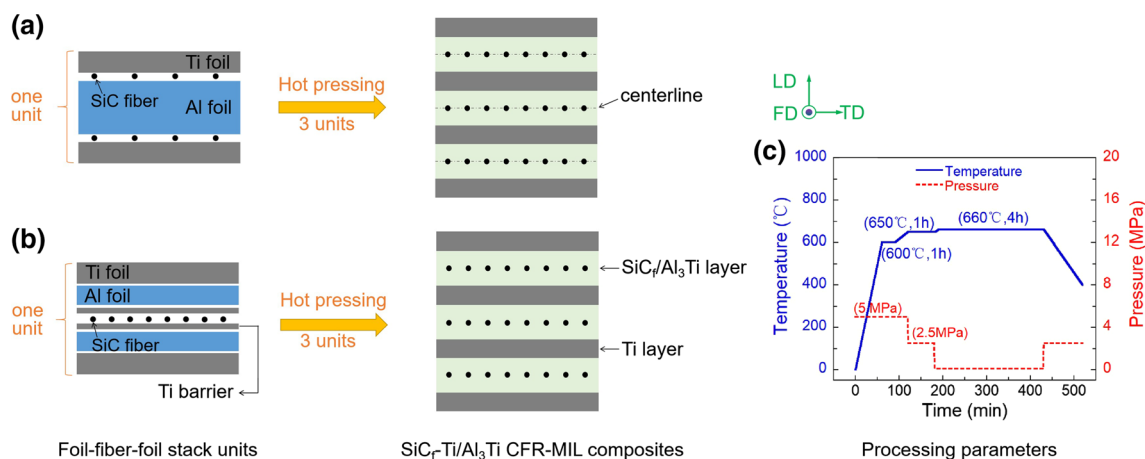


Fig. 1 Schematic illustrations of fabricating $\text{SiC}_f\text{-Ti}/\text{Al}_3\text{Ti}$ CFR-MIL composite: stack units and laminated structures of the non-optimized composite (a) and optimized one (b), vacuum hot pressing processing parameters (c)

reactive sintering are detailed in Fig. 1c. Besides, to analyze the formation mechanism of intermetallic centerline, the microstructure evolution of non-optimized CFR-MIL composite were investigated by interrupting the synthesis reaction in step during sintering.

2.2 Microstructural Characterization

Phase identification of $\text{SiC}_f\text{-Ti}/\text{Al}_3\text{Ti}$ CFR-MIL composite was conducted by X'Pert PRO X-ray diffraction (XRD) from 20° to 90° with the scan speed of $5^\circ/\text{min}$. The microstructure characterization was performed on Hitachi S-3400 scanning electron microscopy (SEM) coupled with energy dispersive spectroscopy (EDS) and electron back-scattered diffraction (EBSD) apparatus. The principal directions of $\text{SiC}_f\text{-Ti}/\text{Al}_3\text{Ti}$ geometry were denoted as the loading direction (LD) of laminates during sintering, its transverse direction (TD), and the fiber axial direction (FD), as indicated in Fig. 1. Additionally, the volume fractions of Ti layers and SiC fibers in $\text{SiC}_f\text{-Ti}/\text{Al}_3\text{Ti}$ composite were calculated by Eqs. 1 and 2, respectively.

$$f_{T1} = \frac{N_{Ti} \cdot T_{Ti}}{N_{Ti} \cdot T_{Ti} + N_{Al_3Ti} \cdot T_{Al_3Ti}} \quad (1)$$

$$f_{SiC} = \frac{N_{SiC} \cdot \pi \cdot (R_{SiC})^2}{(N_{Ti} \cdot T_{Ti} + N_{Al_3Ti} \cdot T_{Al_3Ti}) \cdot W} \quad (2)$$

where the N_{SiC} , N_{Ti} and N_{Al_3Ti} are the number of SiC fibers, Ti layers and Al_3Ti layers, respectively; the T_{Ti} , T_{Al_3Ti} , R_{SiC} and W are the thickness of Ti and Al_3Ti layers, the average radius of SiC fibers and the width of the laminate, respectively.

2.3 Microhardness Tests

The hardness profiles of the Al_3Ti intermetallic with and without centerline in $\text{SiC}_f\text{-Ti}/\text{Al}_3\text{Ti}$ CFR-MIL composite were measured using a microhardness tester by Vickers indentation, respectively. The hardness tests were performed under an indentation load of 200 g for 15 s. Analysis points were spaced so as to eliminate the effect of neighboring indentations. After testing, the appearances of rhomboid indentations were observed by SEM.

2.4 Compression Tests

To analyze the mechanical behaviors of the optimized and non-optimized $\text{SiC}_f\text{-Ti}/\text{Al}_3\text{Ti}$ CFR-MIL composites, quasi-static compression tests were carried out on Instron 5500R load frame at a strain rate of $\sim 0.001/\text{s}$ under room temperature. The loading was perpendicular to layers and fiber orientation of the CFR-MIL composite. The dimensions of the specimens were $6 \text{ mm} \times 6 \text{ mm} \times 6 \text{ mm}$. Before testing, the specimens were ground from 600 to 2000 grit, and then carefully polished. The test was repeated five times for each composite in order to evaluate the corresponding mechanical properties. The compressive strength and failure strain were derived from the measured engineering stress and strain data. After tests, the fracture surfaces of compression specimens were observed by SEM.

3 Results

3.1 Microstructure Characterization

Figure 2 illustrates the XRD patterns of $\text{SiC}_f\text{-Ti}/\text{Al}_3\text{Ti}$ ceramic-fiber-reinforced metal-intermetallic-laminated

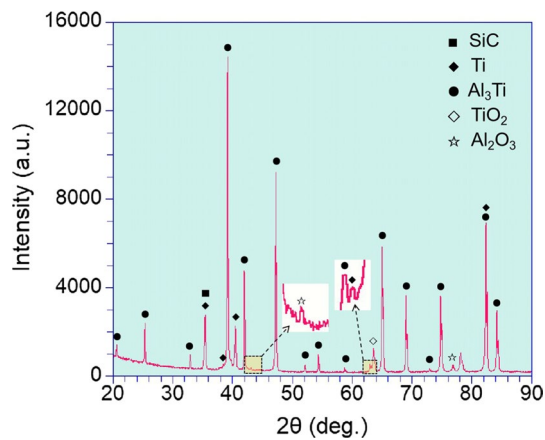


Fig. 2 XRD patterns of $\text{SiC}_f\text{-Ti}/\text{Al}_3\text{Ti}$ CFR-MIL composite prepared using Ti- $\text{SiC}_f\text{-Al}$ stacks

(CFR-MIL) composite fabricated via vacuum hot pressing using Ti foils, Al foils and SiC fibers as raw materials. It can be seen that the CFR-MIL composite mainly consists of SiC fibers, Al_3Ti and Ti phases, as well as some metallic oxides (Al_2O_3 and TiO_2) that might be originated from the surfaces of raw foils. Besides, the XRD patterns reveals that all Al phases were consumed by Ti–Al diffusion reaction to form intermetallic Al_3Ti during sintering process.

Figure 3 shows the typical microstructure of $\text{SiC}_f\text{-Ti}/\text{Al}_3\text{Ti}$ CFR-MIL composite prepared using three primary Ti- $\text{SiC}_f\text{-Al-SiC}_f\text{-Ti}$ units (see Fig. 1a). As presented in Fig. 3a, the reaction synthesis results in laminated microstructure with alternative fiber-reinforced intermetallic layers ($\text{SiC}_f/\text{Al}_3\text{Ti}$) and titanium layers. In this non-optimized CFR-MIL composite, the volume fractions of Ti layers and SiC fibers are 25% and 0.5%, respectively. Moreover, it can be observed from Fig. 3b that SiC fibers are arranged regularly in the

mid-plane of Al_3Ti phase, where numerous micro voids exist as incompletely continuous gaps. Actually, these defects comprise the intermetallic centerline of $\text{SiC}_f\text{-Ti}/\text{Al}_3\text{Ti}$ CFR-MIL composite, as reported by previous work [20].

Figure 4 shows the SEM image and the corresponding EDS analysis results of Zone A (marked in Fig. 3b), presenting the microstructure and component elements of $\text{SiC}_f/\text{Al}_3\text{Ti}$ interfacial region in $\text{SiC}_f\text{-Ti}/\text{Al}_3\text{Ti}$ CFR-MIL composite. It is noted in Fig. 4a that the centerline is clearly observed near SiC fiber. In addition, the concentrated oxygen atoms, as well as a small amount of Al and Ti atoms, are detected at centerline region, as shown in Fig. 4b–f. Apparently, the oxide inclusions identified by XRD analysis, including Al_2O_3 and TiO_2 are mainly distributed along intermetallic centerline. Thus, it is reasonable to guess that there may be relationship between the formation of intermetallic centerline and the accumulation of metallic oxides. This phenomenon will be analyzed in the following discussion part about the formation mechanism of intermetallic centerline in CFR-MIL composite in this work. Furthermore, Fig. 4g indicated the contents of traced elements in Area I (marked in Fig. 4a). It can be seen that the ration of Al/Ti atoms in Area I is approximately 3:1 regardless of the elements V (~ 0.27 at%) and O (~ 2.23 at%), revealing that Al_3Ti is the only Ti–Al binary intermetallic in the CFR-MIL composite [22]. Additionally, the content fluctuation trends of elements across the $\text{SiC}_f/\text{Al}_3\text{Ti}$ interface reflected that the elements (Ti, Al, Si, C) were diffused at the interfacial zone with a quite short distance (< 1 μm) and a small amount (< 3 at%), as shown in Fig. 4h. It should be pointed out that element C was not detected accurately by EDS line analysis, which was consistent with the literature [12], while the results of EDS point scan (Fig. 4a) indicated that only few C atoms were diffused from SiC fiber to the interfacial zone, as listed in Table 1. Besides, an obvious circular gap

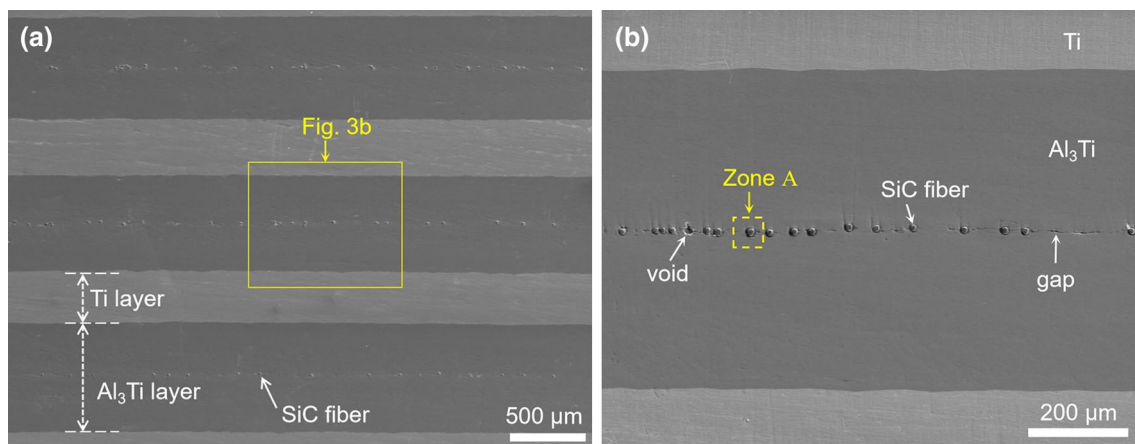


Fig. 3 The SEM images of $\text{SiC}_f\text{-Ti}/\text{Al}_3\text{Ti}$ CFR-MIL composite prepared using Ti- $\text{SiC}_f\text{-Al-SiC}_f\text{-Ti}$ stacks: **a** the typical laminated structure, **b** the microstructure of intermetallic layer

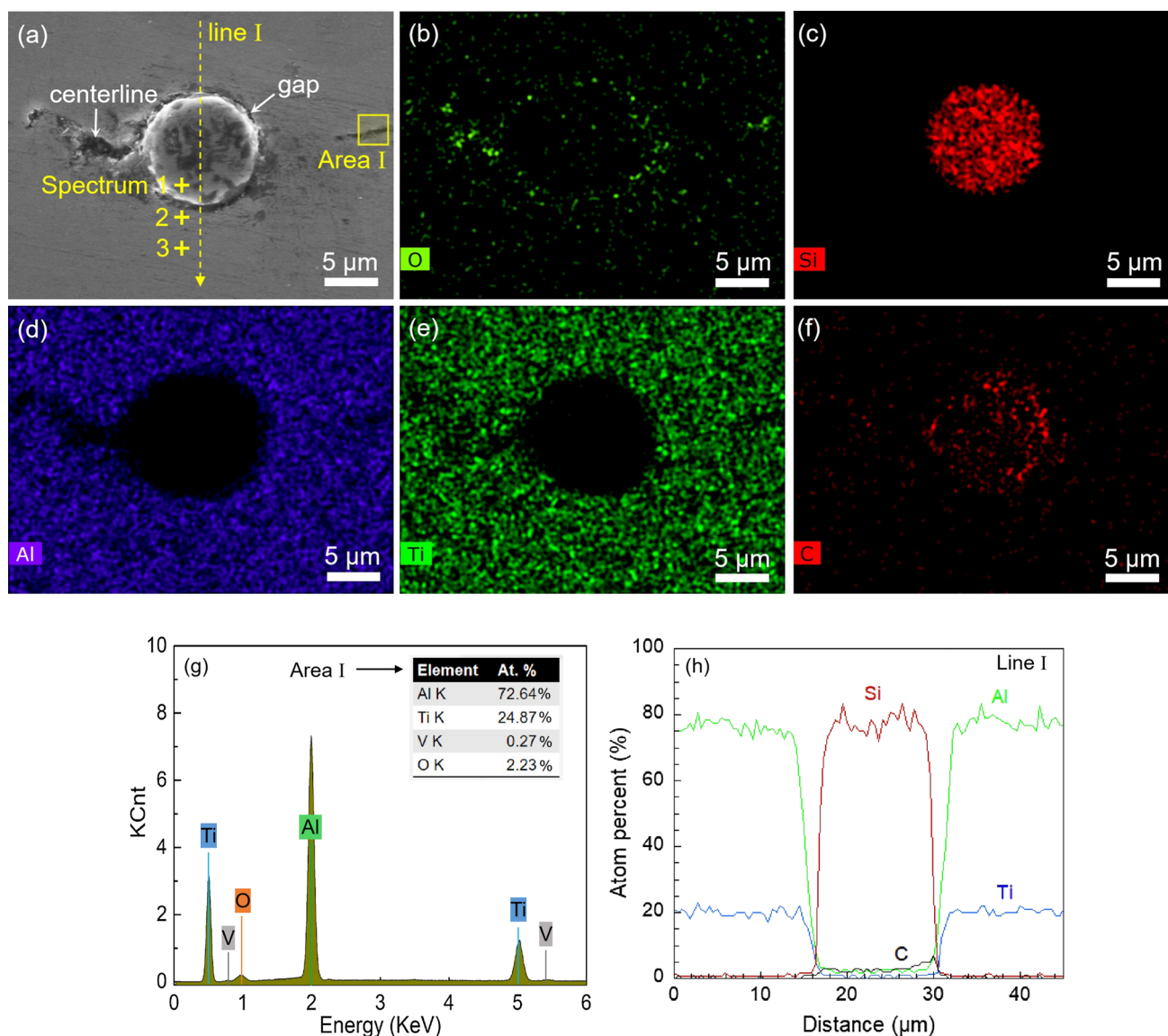


Fig. 4 Microstructure analysis results of Zone A marked in Fig. 3b: **a** SEM image, **b–f** element distribution maps of O, Si, Al, Ti and C, respectively, **g** element contents in Area I, **h** content fluctuation of elements along line I

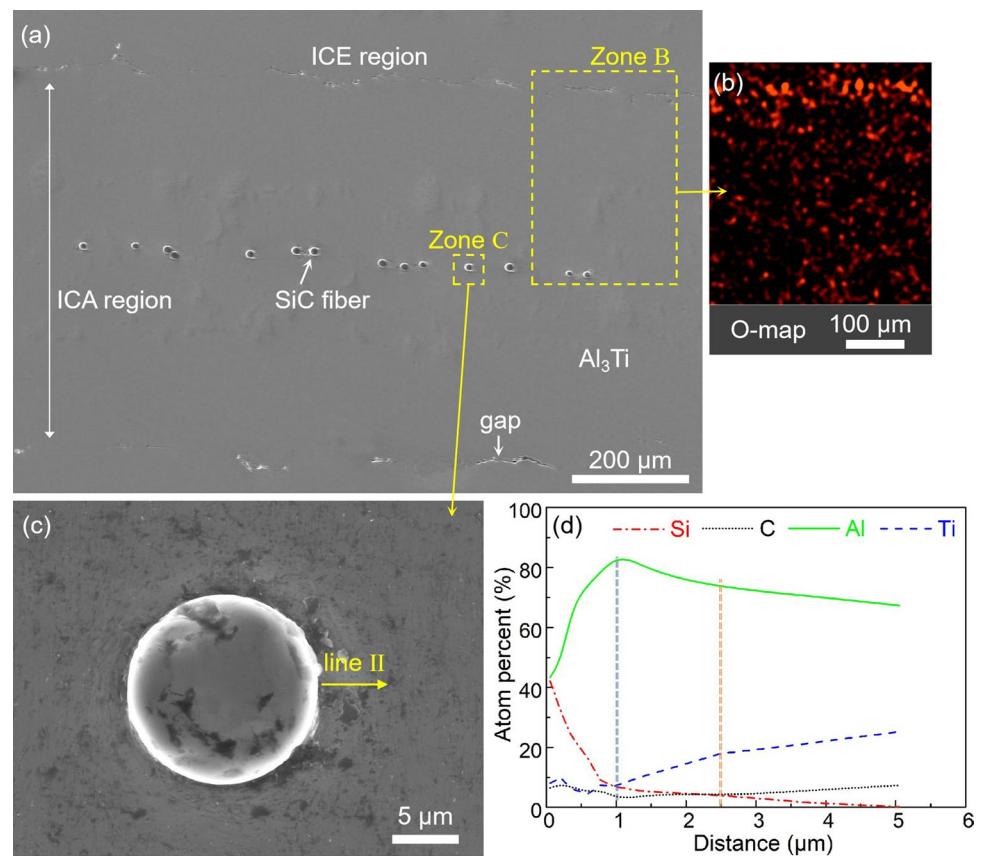
Table 1 Typical chemical compositions of the $\text{SiC}_f/\text{Al}_3\text{Ti}$ interfacial zone detected by EDS

Number	Composition (at%)				Components
	Si	C	Al	Ti	
Spectrum 1	43.2	56.8	–	–	SiC fiber
Spectrum 2	1.2	2.9	69.8	26.1	Interfacial zone
Spectrum 3	–	–	74.3	25.7	Al_3Ti phase

can be found around SiC fiber of the CFR-MIL composite in Fig. 4a. All these phenomena implied the poor interfacial bonding between SiC fiber and Al_3Ti intermetallic, which is caused by the co-existed centerline.

It is known that well-bonded interface can transfer load effectively from matrix to fiber, improving the mechanical properties of fiber reinforced composite due to fiber pull-out, bridging and interface debonding [23, 24]. Thus, it is necessary to improve the bonding of $\text{SiC}_f/\text{Al}_3\text{Ti}$ interface in CFR-MIL composite. In order to obtain structure-optimized $\text{SiC}_f\text{-Ti}/\text{Al}_3\text{Ti}$ CFR-MIL composite, an optimal stack unit of “ $\text{Ti-Al-Ti}_{\text{barrier}}\text{-SiC}_f\text{-Ti}_{\text{barrier}}\text{-Al-Ti}$ ” is designed through introducing thin titanium sheet as barrier layer between SiC fiber and Al foil. Figure 5 presents the microstructure of Al_3Ti intermetallic layer in the optimized CFR-MIL composite. It can be obviously seen from Fig. 5a that a dense $\text{SiC}_f/\text{Al}_3\text{Ti}$ region is achieved, from which intermetallic centerline is absent (marked as ICA region). This indicates that SiC fiber

Fig. 5 **a** The microstructure of $\text{SiC}_f/\text{Al}_3\text{Ti}$ layer in optimized CFR-MIL composite prepared using $\text{Ti-Al-Ti}_{\text{barrier}}\text{-SiC}_f\text{-Ti}_{\text{barrier}}\text{-Al-Ti}$ stacks, **b** oxygen element distribution map of Zone B, **c** the magnified SEM image of Zone C, **d** EDS analysis result along line II



is successfully separated from the centerline in optimized CFR-MIL composite due to the introducing of Ti barrier layer. Moreover, gaps are distributed at the region that is far from the mid-plane of Al_3Ti layer, forming smaller intermetallic centerline existing (ICE) region. Furthermore, it is worth noting from Fig. 5b that oxygen atoms mainly concentrate in the ICE region of $\text{SiC}_f/\text{Al}_3\text{Ti}$ layer. There is no O-rich area appearing around SiC fiber as well as other part of the ICA region. Besides, void cannot also be found at the $\text{SiC}_f/\text{Al}_3\text{Ti}$ interfacial zone (Fig. 5c). Figure 5d shows the elemental compositions of $\text{SiC}_f/\text{Al}_3\text{Ti}$ interface determined via EDS line scan (line II). It can be noticed that Si and C atoms diffuse from SiC fiber to intermetallic layer with a distance of $\sim 5 \mu\text{m}$. Due to the diffusion of Si, C, Al and Ti atoms, a strong metallurgical bonding occurs between SiC fiber and Al_3Ti matrix. The reaction species of the interface have been investigated detailedly via EDS and XRD analysis in previous works [12, 14, 25]. In light of this, it can draw a conclusion that the addition of Ti barrier improves the $\text{SiC}_f/\text{Al}_3\text{Ti}$ interfacial bond of the optimized CFR-MIL composite effectively.

In summary, the intermetallic centerline zone mainly contains micro voids and metallic oxides, both of which have negative influence on the interfacial bonding between SiC fiber and Al_3Ti matrix in $\text{SiC}_f\text{-Ti}/\text{Al}_3\text{Ti}$ CFR-MIL composite without structural optimization. However, the $\text{SiC}_f/$

Al_3Ti interface of the CFR-MIL composite is successfully improved by adding Ti barrier layer between SiC fiber and Al phase before sintering. Therefore, SiC fiber can provide enough strengthening and toughening effect owing to the strong metallurgical bonding of $\text{SiC}_f/\text{Al}_3\text{Ti}$ interface achieved in the optimized CFR-MIL composite.

3.2 Mechanical Properties

The effect of centerline defects on mechanical performance of Al_3Ti phase in $\text{SiC}_f\text{-Ti}/\text{Al}_3\text{Ti}$ CFR-MIL composite was studied by microhardness tests. Figure 6 shows the morphological images of indentations in Al_3Ti phase after testing. It can be seen that the shape and size of indentations are uniform in dense Al_3Ti area, indicating that Al_3Ti phase in ICA region possesses a uniform microstructure and stable hardness. On the contrary, the sizes of indentations in ICE region are usually fluctuated, suggesting variable hardness values ranging from 245 to 512 HV, as listed in Table 2. Thus, there is no point in calculating the mean hardness for porous Al_3Ti phase. Moreover, it is significant to note that the dense Al_3Ti intermetallic shows relatively higher hardness (average ~ 526 HV) than those of Al_3Ti phase with voids. Obviously, intermetallic centerline is a weak area of Al_3Ti phase in CFR-MIL composites.

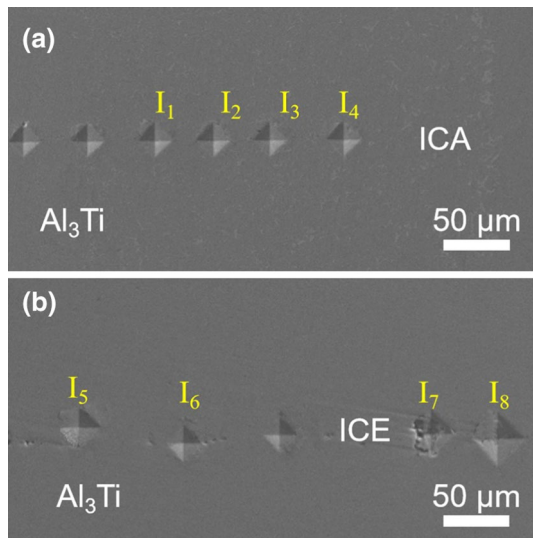


Fig. 6 Indentations of microhardness tests in ICA (a) and ICE (b) regions

To investigate the influence of structural optimization on the mechanical properties and failure behavior of CFR-MIL composite, quasi-static compression tests were performed with the load perpendicular to layers. Figure 7 shows typical compression stress–strain curves of the optimized and the non-optimized CFR-MIL composites. As seen, both of these two curves contains an initial elastic stage and the following plastic deformation stage until a sudden drop of stress, which suggests the fracture of laminates with the increase of load. Besides, it is clearly noted from Table 3 that compression strength (σ_c) and failure strain (ϵ_f) of the optimized CFR-MIL composite are ~ 1412 MPa and 4.1%, respectively, both of which are higher than those (σ_c : 1358 MPa, ϵ_f : 3.6%) of the non-optimized CFR-MIL composite. It indicates that the optimized microstructure benefits mechanical performances of the CFR-MIL composite, including compressive strength as well as ductility. In addition, it can be seen from Fig. 7 that area of the region between strain axis and the compression stress–strain curve of optimized CFR-MIL composite is higher than that of the non-optimized composite. This phenomenon reveals that the optimized $\text{SiC}_f\text{-Ti}/\text{Al}_3\text{Ti}$ CFR-MIL composite possesses superior toughness as compared to the CFR-MIL composite without structural optimization.

Table 2 Microhardness values of Al_3Ti phases in dense ICA and porous ICE regions

Region	Indentation	Hardness (HV)	Region	Indentation	Hardness (HV)
ICA	I ₁	520	ICE	I ₅	453
	I ₂	536		I ₆	512
	I ₃	526		I ₇	245
	I ₄	522		I ₈	257
	Average	526		Average	-

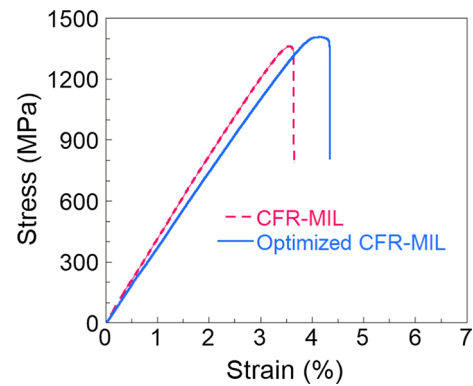


Fig. 7 The typical compression stress–strain curves of the optimized and non-optimized CFR-MIL composites

Table 3 Compression properties of the optimized and non-optimized CFR-MIL composites

Materials	Specimens#	Compressive strength (MPa)	Failure strain (%)
Optimized $\text{SiC}_f\text{-Ti}/\text{Al}_3\text{Ti}$	1	1409	4.3
	2	1433	4.1
	3	1401	4.1
	4	1413	3.9
	5	1404	4.2
	Ave	1412	4.1
Non-optimized $\text{SiC}_f\text{-Ti}/\text{Al}_3\text{Ti}$	1	1363	3.7
	2	1344	3.6
	3	1327	3.4
	4	1384	3.7
	5	1372	3.5
	Ave	1358	3.6

Thus, it can be drawn the conclusion that due to the adding of Ti barrier, both the strength and toughness of $\text{SiC}_f\text{-Ti}/\text{Al}_3\text{Ti}$ CFR-MIL composites are improved effectively.

To understand the fracture mechanisms of $\text{SiC}_f\text{-Ti}/\text{Al}_3\text{Ti}$ CFR-MIL composites with and without structural optimization, the fractured surfaces of compression specimens were observed by SEM. Figure 8 illustrates the fracture micrographs of non-optimized $\text{SiC}_f\text{-Ti}/\text{Al}_3\text{Ti}$ composite. It can be seen that Al_3Ti intermetallic exhibits brittle fracture

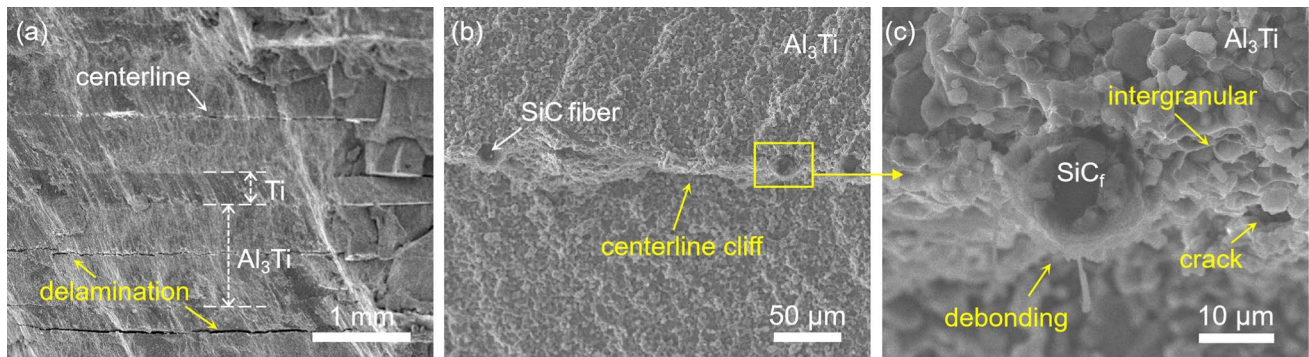


Fig. 8 The fracture surfaces of the CFR-MIL composite without structural optimization: **a** the overall fracture morphology, **b** the fracture mode of intermetallic centerline region, **c** indicating the fracture feature of $\text{SiC}_f/\text{Al}_3\text{Ti}$ interfacial zone

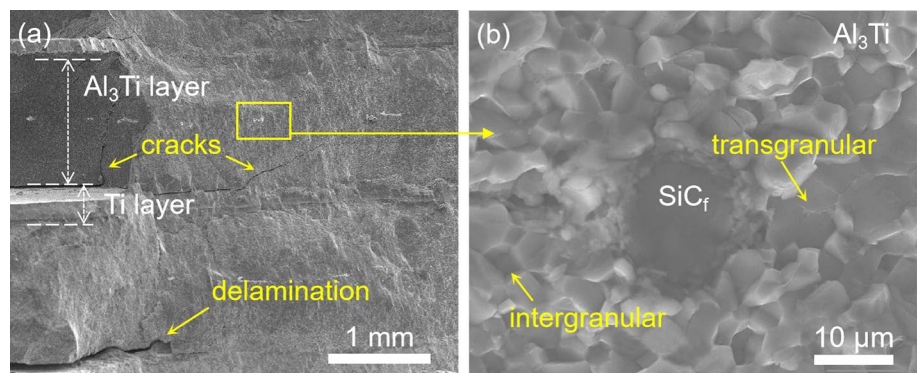
with intergranular mode. Besides, delamination behaviors occur not only at $\text{Ti}/\text{Al}_3\text{Ti}$ interfacial zone, but also along the intermetallic centerline (Fig. 8a). The similar phenomenon has been found in previously reported work [14]. The centerline delamination with cliff structure leads to the untimely debonding between SiC fiber and Al_3Ti intermetallic, as shown in Figs. 8b and c. Clearly, it is difficult for SiC fibers to enhance the properties of CFR-MIL composite via fiber bridging mechanism [26, 27]. Figure 9 shows the fracture morphologies of the optimized CFR-MIL specimens. The intermetallic Al_3Ti near SiC fiber is failed with various brittle fracture types, including transgranular and intergranular modes. Additionally, most cracks propagate along the $\text{Ti}/\text{Al}_3\text{Ti}$ interfacial zone, and few cracks extend with the orientation parallel to layers (Fig. 9a), indicating that no centerline delamination occurs in the optimized CFR-MIL composite. In addition, SiC fibers are still bonded well with Al_3Ti matrix, as can be seen in Fig. 9b. Thus, it can be sum up as that the mechanical performances of $\text{SiC}_f\text{-Ti}/\text{Al}_3\text{Ti}$ CFR-MIL composite are effectively improved due to the optimized microstructure that promotes the strengthening and toughening effects of SiC fibers.

4 Discussion

4.1 Formation Mechanism of Intermetallic Centerline

In the present work, non-optimized $\text{SiC}_f\text{-Ti}/\text{Al}_3\text{Ti}$ CFR-MIL composite was prepared via the vacuum hot pressing sintering using “ Ti-SiC-Al-SiC-Ti ” stacks. The results derived from Figs. 3, 4 and 5 indicated that reaction between solid Ti and liquid Al at 660°C for 4 h resulted in the formation of intermetallic centerline at mid-plane of Al_3Ti layer, which was composed of micro voids and metallic oxides. In order to clarify the forming mechanism of intermetallic centerline, the microstructure evolution of the CFR-MIL composite during sintering was tracked by interrupting the progression of synthesis reaction, including Ti/Al solid–solid and solid–liquid reactions in sequence. In this section, SiC fiber with larger diameter ($\sim 85\ \mu\text{m}$) were employed for easily observing its migration behavior. Figure 10 presents the cross-sectional micrographs of CFR-MIL composite obtained at various stages of reaction synthesis. It can be seen from Fig. 10a that after sintering at 650°C under 2.5 MPa for 1 h, a continuous and dense Al_3Ti intermetallic layer ($\sim 4\ \mu\text{m}$ thick) was formed between solid Al and Ti foils due to the

Fig. 9 The fracture morphologies of the optimized CFR-MIL composite: **a** the overall fracture morphology, **b** the fracture mode of $\text{SiC}_f/\text{Al}_3\text{Ti}$ interfacial zone



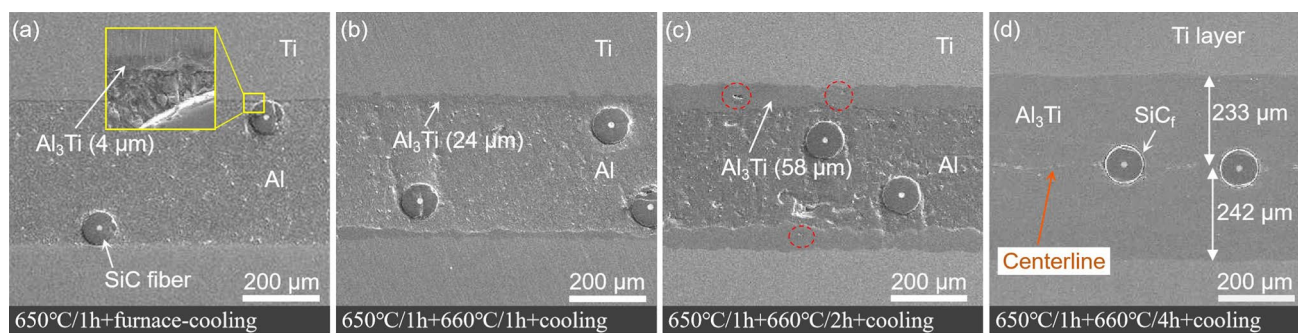


Fig. 10 Microstructures of the CFR-MIL laminates prepared using Ti-SiC_f-Al-SiC_f-Ti stack by reaction synthesis at: **a** 650 °C/1 h, **b** 650 °C/1 h + 660 °C/1 h, **c** 650 °C/1 h + 660 °C/2 h, **d** 650 °C/1 h + 660 °C/4 h

thermodynamically favored reaction “Ti + 3Al → Al₃Ti” [28–30]. At this stage, SiC fibers were mainly distributed at Al/Al₃Ti interface front. Subsequently, the reaction temperature was raised to 660 °C, and the pressure was removed to avoid the expulsion of molten Al phase. The rising of temperature accelerated the diffusion of Ti and Al atoms through intermetallic layer. After reaction at 660 °C for 1 h, the mean thickness of Al₃Ti layer was increased to ~24 μm, as shown in Fig. 10b. It is obvious that the thickening rate of Al₃Ti layer was significantly increased by ~5 times attributed to the faster interdiffusion reaction “Ti(s) + 3Al(l) → Al₃Ti(s)”. During this period, SiC fibers began to move away from Al/Al₃Ti interface to liquid Al phase. When the reaction time was prolonged to 2 h, the Al/Al₃Ti interface migrated gradually towards the middle part of original Al foil. As a result, the Al₃Ti layer became thicker (~58 μm), and some microvoids were formed, as marked with red circles in Fig. 10c. Besides, SiC fiber moved progressively toward the center part of liquid Al phase, rather than in the front of intermetallic layer. The microstructure of CFR-MIL composite synthesized at 660 °C for 4 h are displayed in Fig. 10d. It can be observed that Al phase was completely consumed and the CFR-MIL composite was consisted of three main

components: unreacted Ti and newly-formed Al₃Ti layers, as well as SiC fibers in intermetallic layer. As forecasted, centerline defect was found at the mid-plane of intermetallic layer, accompanying with SiC fiber reinforcement.

According to the microstructure evolution of CFR-MIL composite, it can be deduced that the formation of intermetallic centerline involves three stages, as schematically illustrated in Fig. 11. Initially, Ti and Al atoms inter-diffused towards each other (solid state), causing the dissolution of Ti into Al(Ti) solid solution, as well as Al into Ti(Al) solid solution. When supersaturated, Al₃Ti grains nucleated at Ti/Al interface, and then merged into a continuous layer. The microstructure of this intermetallic layer is dense, due to the applied pressure and the slow diffusion of Ti and Al atoms. Besides, SiC fibers and metallic oxides were pushed into the softened Al phase near intermetallic layer. In the second stage (660 °C), Ti and Al atoms must diffuse through intermetallic layer before reactions occurred at Al/Al₃Ti and Ti/Al₃Ti interfaces. According to Kirkendall effect, when Ti and Al materials were placed next to each other, diffusion between them took place based on the substitution with vacancy [31, 32]. Atoms can switch places with vacancies by moving into vacant lattice sites, making a flux of atoms in one direction and

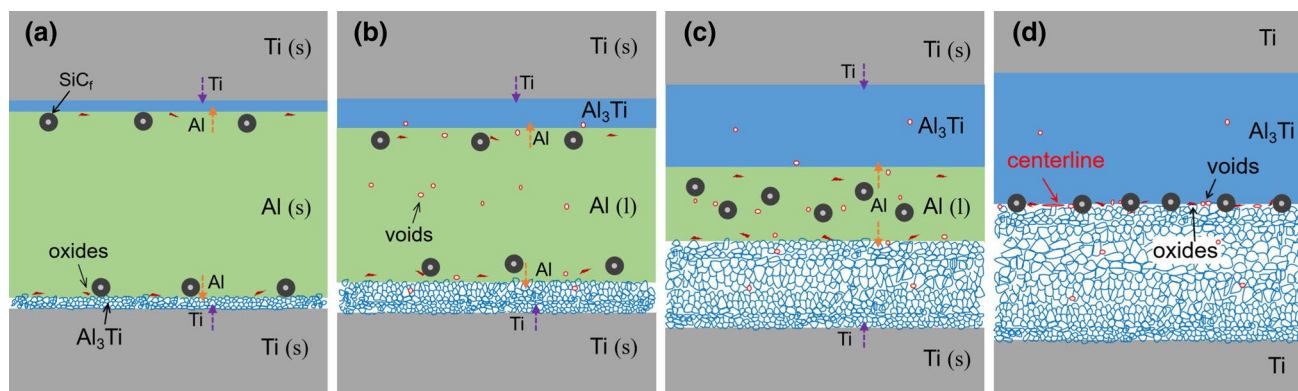


Fig. 11 Schematic illustrations of the formation process of CFR-MIL composite synthesized using Ti-SiC_f-Al-SiC_f-Ti stack: **a** Ti-Al solid-state reaction process, **b** and **c** solid-liquid reaction process, **d** the laminated composite after hot pressing sintering process

a flux of vacancies in the other. In fact, for Ti/Al diffusion couple, the net migration of atoms was from Al layer towards Ti layer, because of the higher diffusion coefficient of Al atom in Al_3Ti phase compared to Ti atom. Thus, vacancies will diffuse along the direction from Ti layer to Al layer and accumulate in Al_3Ti phase closed to Al/ Al_3Ti interface. In addition, as the diffusion of Al atoms towards the interface, the original spots of Al atoms were empty, which led to the formation of vacancies in Al phase near the Al/ Al_3Ti interface. In addition, due to the supplement of Al atoms diffused from farther region of Al phase, only few vacancies were left in Al and Al_3Ti phases closed to their interface. While in the farther region of Al phase (i.e. the middle of Al phase), vacancies could not be filled, resulting in the maximum number of vacancies in the center of Al phase. With the increasing of reaction time, Al_3Ti layer grew thicker with the direction perpendicular to layers. Moreover, vacancies aggregated to form numbers of micron-sized voids in Al_3Ti and Al phases that were without pressure. The voids in liquid Al phase moved towards the center zone of Al layer, while the ones in Al_3Ti phase were fixed. Additionally, SiC fibers and metallic oxides concentrated progressively toward the center part of liquid Al phase, rather than stayed at the Al/ Al_3Ti interfacial zone. Finally, after liquid Al phase was consumed completely (Fig. 11d), the reaction interface of Al/ Al_3Ti moving from one Ti layer met the corresponding interface moving from the next layer at the mid-plane of original Al foils. Numbers of micro voids left from Al phase connected to other ones and coalesced into discontinuous gaps in the middle of Al_3Ti layer, forming the intermetallic centerline defect. Similar parallel cracks were discovered in Ti/ Al_3Ti laminated composite fabricated via self-propagating synthesis [5, 29]. Besides, Sun et al. [33] also found that the voids were distributed at the middle of NiAl intermetallic prepared via reaction synthesis of layered Ni/Al foils. However, Konieczny et al. [34] and Wang et al. [35] attributed the formation of centerline to the accumulated oxide inclusions in the middle of intermetallic layer of MIL composites. In the present work, metallic oxides originating from the surface of initial foils were also detected along the centerline by XRD and EDS (Figs. 3, 4 and 5). It indicated that the centerline are possibly comprised of the micro voids formed by Kirkendall effect and the residual oxides originated from surface of metal foils. Therefore, it can draw a conclusion that the intermetallic centerline in $\text{SiC}_f\text{-Ti}/\text{Al}_3\text{Ti}$ CFR-MIL composite is a product of the synthesis method, the original material state, the Ti–Al diffusion reaction mechanism and the reaction kinetics.

4.2 Optimization Mechanisms of Microstructure and Properties

It was demonstrated that SiC fiber and centerline defect are always distributed in the mid-plane of intermetallic layer in CFR-MIL composite, and their co-existence weakens

the interfacial bonding between fiber reinforcement and intermetallic matrix. In the present work, a structure-optimized $\text{SiC}_f\text{-Ti}/\text{Al}_3\text{Ti}$ CFR-MIL composite with a dense $\text{SiC}_f/\text{Al}_3\text{Ti}$ region has been fabricated through adding Ti barrier sheet into initial stacks (Fig. 5). In addition, the compressive strength and toughness of CFR-MIL composite are improved significantly owing to the structural optimization (Fig. 7). For investigating the optimization mechanism accurately, EBSD analysis was performed to characterize the microstructure of $\text{SiC}_f/\text{Al}_3\text{Ti}$ layer in the CFR-MIL composite prepared using “Ti–Al–Ti barrier/ SiC_f/Ti barrier–Al– $\text{SiC}_f\text{-Ti}$ ” multi-stacks (insert of Fig. 12a). Figure 12 displays the corresponding results of EBSD analysis, including micro appearance, grain morphology, distribution maps of grain size and crystal orientation. As can be seen in Fig. 12a, $\text{SiC}_f/\text{Al}_3\text{Ti}$ layer are composed of dense ICA region and porous ICE region, which are formed from Al– $\text{Ti}_{\text{barrier}}\text{-SiC}_f\text{-Ti}_{\text{barrier}}\text{-Al}$ and Al– $\text{SiC}_f\text{-Ti}$ ” parts of the multi-stacks, respectively. Besides, SiC fibers in ICA region are well-bonded with dense Al_3Ti intermetallic, while the fibers in the ICE region are surrounded with numerous voids. Apparently, the improved microstructure of Al_3Ti phase is obtained attributed to the addition of Ti barrier layer. Moreover, it is noted from Fig. 12b that the inverse pole figure (IPF) map of $\text{SiC}_f/\text{Al}_3\text{Ti}$ layer contains identified zones of Al_3Ti phase and unidentified zones of SiC fiber. The area of unrecognized hole in ICE region is much bigger than that in ICA region, indicating the existence of voids around SiC fibers in ICE region. Additionally, individual grains are colored in the IPF map according to their crystallographic orientations relative to loading direction (LD) during sintering. Remarkably, Al_3Ti grains in ICE region exhibit similar orientation ($\{001\}/\text{LD}$) according to the narrow variation of colors between them, while no texture is developed in ICA region. This is related to the metallic oxides distributed along centerline in ICE region. The pole figures of Al_3Ti grains (Fig. 12c) derived from the whole intermetallic layer show the same result that the textures of Al_3Ti grains are almost scattered with the maximum pole intensity of 1.39, since the Al_3Ti grains with random crystal orientation covers most areas (ICA) of intermetallic layer. Figure 12d and e depict the phase maps of Al_3Ti intermetallic, in which high angle grain boundaries (HAGBs) and low angle grain boundaries (LAGBs) are illustrated by black and red lines, respectively. As seen, the HAGBs dominate in Al_3Ti grains of both ICA and ICE regions. Nevertheless, the Al_3Ti grains exhibit differences of morphology, distribution and size between these two regions. The Al_3Ti phase in ICA region is made of numerous nearly-equiaxed fine grains, as well as a few equiaxed and elongated coarse grains surrounded by these fine grains. The average diameter of Al_3Ti grains in ICA

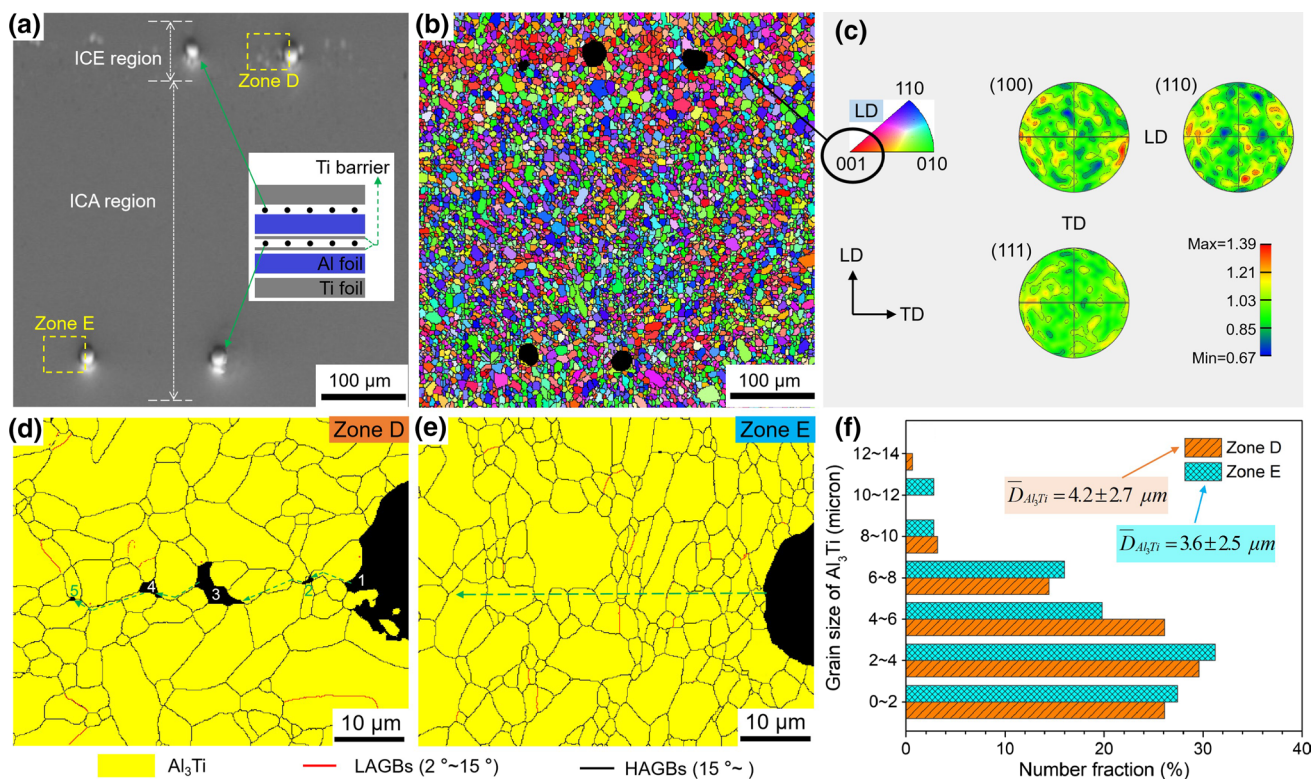


Fig. 12 EBSD analysis results of SiC_f-Ti/Al₃Ti CFR-MIL composite fabricated using multi-stacks: **a** micrograph of SiC_f/Al₃Ti layer, **b** corresponding IPF distribution map, **c** pole figures of Al₃Ti inter-

metallic, **d** and **e** phase maps of Zone D and Zone E, respectively, and **f** statistical charts of Al₃Ti grain size in these two zones

region is 3.6 μm , which is smaller than that (4.2 μm) of ICE region, as shown in Fig. 12f. Moreover, fine equiaxed and coarse elongated grains cover the most area of Al₃Ti phase in ICE region, except for the zone occupied by micro voids that take a limited proportion. While there is no evidence of micro voids found in ICA region, which further reflects that the centerline defect is mainly formed in the region where Al liquid is exhausted during hot pressing. Clearly, there is relationship between the formation of Al₃Ti grains and the existence of defects, including oxides and voids in liquid Al, which has been evidenced by Sun et al. [33]. In addition, it is important to note that the voids in ICE region (sites 1–5 in Fig. 12d) are connected by a series of grain boundaries in linear distribution without waves, as marked by green dotted lines with oriented arrow. Thus, when the CFR-MIL composite are loaded, cracks can easily propagate along these voids and grain boundaries in ICE region. Then, fracture occurs along this region, leading to centerline cliff and interfacial debonding between SiC fiber and Al₃Ti intermetallic. This phenomenon has been observed in the compression fracture surface of non-optimized CFR-MIL specimen, as presented in Fig. 8. Unlike that, the extending of cracks in ICA region are realized by intergranular fracture along

tortuous grain boundaries and transgranular mode along the dotted lines marked in Fig. 12e. Additionally, the SiC fiber in this region can restrain the propagation of cracks by bridging due to the metallurgically-bonded SiC_f/Al₃Ti interface. All these behaviors will absorb more energy, improving the mechanical properties, including strength and toughness of the CFR-MIL composite. Similar results have been found in the optimized CFR-MIL composite, as shown in Figs. 7 and 9.

Considering the same sintering condition as well as the identical constituents and pre-treatment of raw materials, it can be confirmed that the differences of microstructure and mechanical behavior between ICA region and ICE region are caused by adding of Ti barrier layer. In fact, there is no mystery as to why Ti barrier placed between SiC fiber and Al foil can improve the microstructure and performances. Based on the above discussion, SiC fibers, Kirkendall voids and metallic oxides possess similar moving trails in molten Al during the process of microstructure evolution. Due to the existence of Ti barrier, the oxides and voids are pushed away from the center part of intermetallic layer and gather in ICE region distributing between ICA region and Al₃Ti phase adjacent to Ti layer. Unlike that, the intermetallic phases between Ti barriers without defects constitute the

ICA region, where SiC fibers are well-bonded with the Al_3Ti matrix. As a result, SiC fibers can strengthen and toughen the optimized CFR-MIL composite through fiber reinforcing mechanisms.

5 Conclusions

In the present work, a novel structure-optimized $\text{SiC}_f\text{-Ti}/\text{Al}_3\text{Ti}$ CFR-MIL composite was successfully fabricated by introducing Ti barrier into initial stack of raw materials. The microstructure evolution and structural optimization mechanism of CFR-MIL composite have been investigated via XRD, SEM and EBSD, and the mechanical properties of CFR-MIL composites have been discussed. The main conclusions drawn from the current work are summarized as follows:

- (1) As a structural weakness of CFR-MIL composite, intermetallic centerline is a product of the synthesis method, the original material state, the Ti–Al diffusion reaction mechanism and kinetics. The centerline region containing metallic oxides and Kirkendall voids is always formed at the mid-plane of Al_3Ti layer, and weakens the bonding of $\text{SiC}_f/\text{Al}_3\text{Ti}$ interface because of the similar moving trail of voids, oxides and fibers in molten Al during hot pressing.
- (2) During sintering, SiC fibers pegged by unmelted Ti barrier sheets are out of touch with liquid Al phase during the whole process of preparing optimized CFR-MIL composite. As a result, SiC fibers are successfully separated from the micro voids and oxide inclusions. Additionally, a metallurgically bonded interface between SiC fiber and Al_3Ti matrix is achieved. Thus, SiC fiber can provide enough strengthening and toughening effects for the brittle intermetallic and the laminated composite.
- (3) The results of quasi-static compression tests indicated that the average compressive strength and failure strain of the optimized CFR-MIL composite are 1412 MPa and 4.1%, respectively, which are obviously improved compared with non-optimized CFR-MIL composite. The reason is that SiC fibers produce enough strengthening effect, and toughen the composite at the same time, which is attributed to the increasing of bonding strength of $\text{SiC}_f/\text{Al}_3\text{Ti}$ interface as a result of the separating of SiC fiber from centerline.
- (4) The observation on compression fracture showed that the non-optimized CFR-MIL composite prefers to fracture along centerline, where cracks can easily propagate through voids and straight grain boundaries. The split of centerline leads to the untimely debonding of $\text{SiC}_f/\text{Al}_3\text{Ti}$ interface. In the optimized CFR-MIL composite,

cracks tend to extend at the interfacial zone between layers instead of cutting off Al_3Ti layer along its mid-plane, which delays the failure of Al_3Ti layer and improves the mechanical properties of the composite.

Acknowledgements The authors gratefully acknowledge the financial supports of this study by the Initial Scientific Research Fund in Changshu Institute of Technology (KYZ2018043Q and KYZ2018044Q).

References

1. W. Sun, F. Yang, F. Kong et al., Interface characteristics of Ti6Al4V-TiAl metal-intermetallic laminate (MIL) composites prepared by a novel hot-pack rolling. *Mater. Charact.* **144**, 173–181 (2018)
2. S. Qin, X. Cui, Z. Tian et al., Synthesis and mechanical properties of innovative (TiB/Ti)- Ti_3Al micro-laminated composites. *J. Alloys Compd.* **700**, 122–129 (2017)
3. Y. Wang, S. Zhou, K.S. Vecchio, Annealing effects on the microstructure and properties of an Fe-based metallic-intermetallic laminate (MIL) composite. *Mater. Sci. Eng. A* **665**, 47–58 (2016)
4. K. Brunelli, L. Peruzzo, M. Dabala, The effect of prolonged heat treatments on the microstructural evolution of Al/Ni intermetallic compounds in multilayered composites. *Mater. Chem. Phys.* **149–150**, 350–358 (2015)
5. M. Yuan, L. Li, Z. Wang, Study of the microstructure modulation and phase formation of Ti- Al_3Ti laminated composites. *Vacuum* **157**, 481–486 (2018)
6. Y. Cao, N. Wei, X. Han et al., Mechanical response of titanium tri-aluminide intermetallic alloy. *Mater. Sci. Eng. A* **706**, 242–248 (2017)
7. I.A. Bataev, A.A. Bataev, V.I. Mali et al., Structural and mechanical properties of metallic-intermetallic laminate composites produced by explosive welding and annealing. *Mater. Des.* **35**, 225–234 (2012)
8. A. Rohatgi, D.J. Harach, K.S. Vecchio et al., Resistance-curve and fracture behavior of Ti- Al_3Ti metallic-intermetallic laminate (MIL) composites. *Acta Mater.* **51**(10), 2933–2957 (2003)
9. F. Jiao, M. Liu, F. Jiang et al., Continuous carbon fiber reinforced Ti/ Al_3Ti metal-intermetallic laminate (MIL) composites fabricated using ultrasonic consolidation assisted hot pressing sintering. *Mater. Sci. Eng. A* **765**, 138225 (2019)
10. J. Liu, L. Zhang, F. Jiang et al., Elasto-plastic mechanical properties and failure mechanism of innovative Ti-($\text{SiC}_f/\text{Al}_3\text{Ti}$) laminated composites for sphere-plane contact at the early stage of penetration process. *Materials* **11**(7), 1152 (2018)
11. Y. Han, C. Lin, X. Han et al., Fabrication, interfacial characterization and mechanical properties of continuous Al_2O_3 ceramic fiber reinforced Ti/ Al_3Ti metal-intermetallic laminated (CCFR-MIL) composite. *Mater. Sci. Eng. A* **688**, 338–345 (2017)
12. C. Lin, Y. Han, C. Guo et al., Synthesis and mechanical properties of novel Ti-($\text{SiC}_f/\text{Al}_3\text{Ti}$) ceramic-fiber-reinforced metal-intermetallic-laminated (CFR-MIL) composites. *J. Alloys Compd.* **722**, 427–437 (2017)
13. K.S. Vecchio, F. Jiang, Fracture toughness of ceramic-fiber-reinforced metallic-intermetallic-laminate (CFR-MIL) composites. *Mater. Sci. Eng. A* **649**, 407–416 (2016)
14. C. Lin, F. Jiang, Y. Han et al., Microstructure evolution and fracture behavior of innovative Ti-($\text{SiC}_f/\text{Al}_3\text{Ti}$) laminated composites. *J. Alloys Compd.* **743**, 52–62 (2018)

15. Y. Chang, Z. Wang, X. Li et al., Continuous Mo fiber reinforced Ti/Al₃Ti metal-intermetallic laminated composites. *Intermetallics* **112**, 106544 (2019)
16. E. Wang, C. Guo, P. Zhou et al., Fabrication, mechanical property and damping capacity of shape memory alloy NiTi fiber-reinforced metal-intermetallic-laminate (SMAFR-MIL) composite. *Mater. Des.* **95**, 446–454 (2016)
17. X. Ma, Q. Zhang, Z. Luo et al., A novel structure of Ferro-Aluminum based sandwich composite for magnetic and electromagnetic interference shielding. *Mater. Des.* **89**, 71–77 (2016)
18. Y. Sun, S.K. Vajpai, K. Ameyama et al., Fabrication of multi-layered Ti-Al intermetallics by spark plasma sintering. *J. Alloys Compd.* **585**, 734–740 (2014)
19. T. Li, F. Jiang, E.A. Olefsky et al., Damage evolution in Ti6Al4V-Al₃Ti metal-intermetallic laminate composites. *Mater. Sci. Eng. A* **443**(1), 1–15 (2007)
20. R.D. Price, F. Jiang, R.M. Kulin et al., Effects of ductile phase volume fraction on the mechanical properties of Ti-Al₃Ti metal-intermetallic laminate (MIL) composites. *Mater. Sci. Eng. A* **528**(7), 3134–3146 (2011)
21. Y. Han, F. Jiang, C. Lin et al., Microstructure and mechanical properties of continuous ceramic SiC and shape memory alloy NiTi hybrid fibers reinforced Ti-Al metal-intermetallic laminated composite. *J. Alloys Compd* **729**, 1145–1155 (2017)
22. L. Peng, J. Wang, H. Li et al., Synthesis and microstructural characterization of Ti-Al₃Ti metal-intermetallic laminate (MIL) composites. *Scrip. Mater.* **52**(3), 243–248 (2005)
23. W. Zhang, Y. Yang, G. Zhao et al., Investigation of interfacial reaction in SiC fiber reinforced Ti-43Al-9V composites. *Intermetallics* **33**, 54–59 (2013)
24. R.O. Ritchie, Mechanisms of fatigue-crack propagation in ductile and brittle solids. *International J. Fract.* **100**(1), 55–83 (1999)
25. D. Zhang, Y. Sun, Y. Zhao et al., Interfacial products in SiC fiber reinforced Ti-Al based intermetallic alloys. *Rare Met.* **30**(1), 524–528 (2011)
26. W. Yu, K. Zhu, Y. Aman et al., Bio-inspired design of SiC_f-reinforced multi-layered Ti-intermetallic composite. *Mater. Des.* **101**, 102–108 (2016)
27. K. Zhu, W. Yu, Y. Aman et al., Synthesis, microstructure and mechanical properties of a bio-inspired Ti-intermetallic multi-layered/SiC_f-reinforced Ti-matrix hybrid composite. *J. Mater. Sci.* **51**(18), 8747–8760 (2016)
28. J. Luo, V.L. Acoff, Using cold roll bonding and annealing to process Ti/Al multi-layered composites from elemental foils. *Mater. Sci. Eng. A* **379**, 164–172 (2004)
29. L. Xu, Y. Cui, Y. Hao et al., Growth of intermetallic layer in multi-laminated Ti/Al diffusion couples. *Mater. Sci. Eng. A* **435–436**, 638–647 (2006)
30. M. Sujata, S. Bhargava, S. Suwas et al., On kinetics of TiAl₃ formation during reaction synthesis from solid Ti and liquid Al. *J. Mater. Sci. Lett.* **20**(24), 2207–2209 (2001)
31. M. Tavooosi, The Kirkendall void formation in Al/Ti interface during solid-state reactive diffusion between Al and Ti. *Surf. Interfaces* **9**, 196–200 (2017)
32. S. Santra, T. Davies, G. Matthews et al., The effect of the size of NbTi filaments on interfacial reactions and the properties of InSn-based superconducting solder joints. *Mater. Des.* **176**, 107836 (2019)
33. Y. Sun, P. Lin, S. Yuan, A novel method for fabricating NiAl alloy sheet components using laminated Ni/Al foils. *Mater. Sci. Eng. A* **754**, 428–436 (2019)
34. M. Konieczny, Mechanical properties and deformation behavior of laminated Ni-(Ni₂Al₃+NiAl₃) and Ni-(Ni₃Al+NiAl) composites. *Mater. Sci. Eng. A* **586**, 11–18 (2013)
35. Y. Wang, K.S. Vecchio, Microstructure evolution in Fe-based-aluminide metallic-intermetallic laminate (MIL) composites. *Mater. Sci. Eng. A* **649**, 325–337 (2016)

Publisher's Note Springer Nature remains neutral with regard to jurisdictional claims in published maps and institutional affiliations.